SIMULATIONS OF TURBULENT MIXING OF TWO FLUIDS WITH VARIABLE ACCELERATION LAWS

A.N. Razin, V.I. Kozlov, I.V. Sapozhnikov
(RFNC – VNIIEF)

Dimonte's experiments have been simulated with the VIKHR technique. The progress of the turbulent mixing zone has been considered resulting from Raleigh-Taylor instability at the interface between two immiscible fluids. The calculations were performed with variable initial turbulent zone width and a sequence of refined grids for increasing, decreasing, pulse and constant accelerations. The turbulent mixing zone growth rate was obtained as a function of the path and initial zone width. It has been shown that the numerical results are in good agreement with the test data.

INTRODUCTION.

At present, the VIKHR technique [1] with V.V. Nikiforov's turbulent mixing (TM) model is widely used in VNIIEF for numerical simulations of flows with turbulent mixing. The Nikiforov's model has been tested many times against TM tests with gases [2-5], including shock tube tests.

Shock tube tests on TM at an interface of two gases with different densities have a number of specific features. First, in these tests, the gases are initially separated by a thin film, which prevents their diffusion before the mixing starts. After the film is ruptured by a shock wave, an initial turbulent mixing zone forms. In this case, the film's mechanical properties have a considerable effect throughout the TM zone evolution. In particular, TM zone width after the test may vary considerably with the film's thickness and strength. Therefore, a physical model that would treat film rupture and the initial phase of TM zone evolution is required for testing turbulent mixing calculation techniques. As such model does not exist, in VIKHR calculations we set initial fluctuations of density. Their values are specified so that to describe the measurements adequately.

Second, TM zone in shock tube tests is formed by means of intense interaction of shock waves and turbulent eddies. In numerical simulations of turbulent flows with

shocks, gas-dynamic gradients at a shock front are inversely proportional to numerical point size. As a result, solutions of TM difference equations are highly dependent on a numerical grid, since gas-dynamic gradients are included in turbulence generation terms of the TM equations.

This is the reason why tests where these uncertainties are absent or insignificant are especially interesting for testing TM numerical techniques. Dimonte's experiments [6] belong to these tests.

In Dimonte's experiments two immiscible fluids were placed in a sealed ampoule: freon ($\rho = 1.57$ g/cm^3) at the bottom and water ($\rho = 1$ g/cm^3) at the top. The interface here is planar, except for the menisci at the ampoule walls due to surface tension that are small compared to the ampoule size. Initial perturbations of the interface are low and result from thermal fluctuations. Interface acceleration resulting into a Raleigh-Taylor instability is caused by the ampoule acceleration by a so-called electric motor (a conductor moving along guide electrodes under the influence of a magnetic field). Four acceleration laws have been obtained by varying the current and magnetic induction in [6]: constant, decreasing, increasing and pulse accelerations. The acceleration was directed from the heavy fluid into the light one.

This paper presents numerical results obtained for the tests [6] with four ampoule acceleration laws. The calculations were performed with the VIKHR technique with the incompressible fluid assumption (as the maximum ampoule velocity is within ~31 м/с, the resulting flow inside the ampoule is definitely subsonic). Surface tension effects were not taken into account.

PROBLEM DEFINITION.

The numerical geometry of the tests [6] is given in the fig. 1. The domain 1 ($0 \le r \le 10$ cm) is filled with water with the density $\rho_1^0 = 1$ g/cm^3, the domain 2 ($10 \le r \le 20$ cm) has liquid freon with the density $\rho_2^0 = 1.57$ g/cm^3. The boundary conditions at the left and right are: rigid wall. In our calculations we used the following equation of state for weakly compressible fluids:

$$P = 1000 + 25[(\rho/\rho_c)^3 - 1]/3,$$

where $\rho_c = \rho_1^0\rho_1^0/(c_1\rho_2^0 + c_2\rho_1^0)$, c_1 and c_2 are the mass fractions of water and freon respectively. In all calculations, the TM zone width was found from the mass fraction levels: c_1=0.02 for the right boundary, c_2=0.02 for the left boundary.

Numerical and experimental results are given as a function $h(Z)$, where h is the depth to which the light fluid penetrates into the heavy one, $Z = \int_0^t dt' \int_0^{t'} dt'' g(t'')$ is the ampoule path ($g(t)$ is the ampoule's variable acceleration). In our calculations we assumed that at small density difference the mixing occurs nearly symmetrically (in [7], for instance, the mixing asymmetry of $\approx 3\%$ was obtained for $\rho_2/\rho_1 \approx 1.5$), so the light-into-heavy fluid penetration depth was found as $h = 0.5(r_1 - r_2)$, where r_1 and r_2 are the coordinates of the right and the left boundaries of the TM zone. For the constant acceleration we also used $S = Z = 0.5gt^2$ for the ampoule's path.

NUMERICAL RESULTS

All calculations were performed with a uniform distribution of numerical points across the domains. The following notation is used in the figures: the first value in brackets is the number of points in the first domain, the second value gives that in the second domain; the notation 1+1 corresponds to initial density fluctuations set in one point at the left and one point at the right from the interface, the notation 2+2 corresponds to initial density fluctuations set in two points to the left and two points to the right from the interface, an so on. The initial density fluctuation in all calculations was set to $R_0 = 0.05$, the initial width of the TM zone was L_0 (the length of the interval where the density fluctuations were set to the non-zero value).

Constant acceleration.

The fig. 2.a and 2.b depict the simulation results for the constant acceleration of the ampoule, the data from [6] are also presented. The fig. 2.a shows that when the grid is refined (which makes the initial TM zone width smaller) the calculations give smaller light-to-heavy fluid penetration depth. So, a twofold increase of the number of points in the differencing grid reduces h at the end of a calculation by about 8%. If we increase the number of points 3-fold, h at the end of a calculation becomes about 12% smaller, and a

4-fold increase makes h at the same time about 14% smaller. The influence of L_0 and the cell linear size is pronounced throughout the calculation, though the ratio $\Delta h/h$ decreases with time.

At the initial phase of TM zone evolution (to $Z \leq 10$) there is a discrepancy between the numerical data and the experiments. In our opinion, this discrepancy can be accounted for by the fluid's interface surface tension, which was not taken into consideration in the calculations (this is also true for the other acceleration laws).

The fig. 2.b present h as a function of L_0. One can see that the dependence of the TM zone growth rate dh/dS on L_0 is most pronounced at the initial phase of the perturbation evolution. With the developed turbulence at $20 < Z < 80$ (in the interval where the ampoule's acceleration is constant) dh/dS shows almost no dependence on L_0:

$$dh/dS \approx 0.0235 \approx 0.11A \tag{1}$$

where $A = (\rho_2 - \rho_1)/(\rho_2 + \rho_1)$ is the Atwood number.

In the references [7÷9] the zone growth rate is to a certain extent dependent on the density level at the left and right boundaries of the TM zone that are used to measure the experimental zone width. For example, the following dependencies are presented in [7] where the TM zone width was found from the dimensionless density profile $\delta = (\rho(x) - \rho_1)/(\rho_2 - \rho_1)$:

$$dh/dS = (0.14 \pm 0.005)A \text{ at } \delta = 1, \tag{2}$$

$$dh/dS = (0.11 \pm 0.01)A \text{ at } \delta = 0.98. \tag{3}$$

(2) and (3) yield at $A = 0.222$ (for the system of water and freon): $dh/dS \approx 0.0244 \div 0.031$, which is higher than the value (1), produced by the VIKHR calculation.

The numerical result (1) and the test data [7÷9] show considerable discrepancies with the dependence derived by Nikiforov [10]:

$$dh/dS = 0.325A, \tag{4}$$

which in our case at $A = 0.222$ yields a noticeably higher TM growth rate $dh/dS \approx 0.072$. The correlation (4) was obtained in TOGA technique calculations and was first given in [10]. The VIKHR calculations performed in the standard manner produced a similar result. According to Nikiforov [11], the reason for these discrepancies between the law (4) and the test data is that the turbulence energy dissipation mechanism, which takes

place when two molecularly immiscible fluids are mixed, is different from that specific for gases.

VIKHR calculations have shown that satisfactory agreement with the test data can be achieved if we introduce a restriction on the function $f_1 = \overline{\rho'^2}/\rho/\rho R$ at the initial phase of a calculation, while preserving the model parameters (all the results, given in this paper were obtained with the restriction on this function). The function f_1 in the Nikiforov's model is a measure of deviation of liquid particles' acceleration from the gas-dynamic acceleration $\nabla P/\rho$, and it is represented as $f_1 = (1 + R - D_t \nabla R/W)^{-1}$. For a heterogeneous mixture of two immiscible fluids there is an analytical expression for this function: $f_1 = \delta[\delta - (\delta - 1)c]^{-2}$, where $\delta = \rho_h/\rho_l$, ρ_h and ρ_l are the densities of the heavy and the light fluid, c is the mass fraction of the light fluid. The value of the function f_1 for an arbitrary turbulent mixture cannot be higher than its heterogeneous value. Meanwhile, the representation of f_1, used in the model at the beginning of TM calculations can result into overestimated f_1. For this reason, a restriction on f_1 is used in calculations, which is equivalent to a restriction on the archimedian forces' work to move the liquid particles. As a result, the turbulence kinetic energy and the turbulent diffusivity decrease, which, in turn, leads to smaller growth of TM zone width. The restriction on the structural function can thus be interpreted as effective consideration of the turbulence energy conversion to the interface surface energy.

Increasing acceleration.

The fig. 3.a, 3.b and 3.c present the numerical results for the increasing acceleration of the ampoule. The fig. 3.a shows that when the grid is refined (which results into a decrease of the initial TM zone width) the light-to-heavy fluid penetration depth slightly decreases. And throughout the calculation h depends on L_0, though the relative change of h decreases with time.

The influence of L_0 on the dependence $h(Z)$ on a fixed grid is shown in the fig. 3.b and 3.c (the data in the fig. 3.c were obtained on a grid with a doubled number of points compared to the fig. 3.b). One can see that when L_0 is changed, it changes $h(Z)$ by a constant value Δh, that is almost independent on the ampoule's path Z. Indeed, the fig. 3.b

shows that at $20 < Z < 70$ the rate of penetration of the light fluid into the heavy one dh/dZ decreases from 0.0314 for $L_0 = 0.02778$ cm to 0.0308 for $L_0 = 0.1111$ cm. If the grid has 2 times more cells (see the fig. 3.c) at $20 < Z < 70$ the value of dh/dZ does not depend on L_0 and equals to 0.0298. This result can be approximated by the dependence

$$dh/dZ \approx 0.135A.$$

Decreasing acceleration.

The numerical results for the decreasing acceleration of the ampoule are given in the fig. 4.a and 4.b. The fig. 4.a shows that an increase of numerical point size results into an increase of TM zone width. At the end of the calculations the light-to-heavy fluid penetration depth is: $h \approx 2.143$ cm on the grid with $L_0 = 0.0833$ cm, $h \approx 1.922$ cm on the grid with $L_0 = 0.0417$ cm, $h \approx 1.831$ cm on the grid with $L_0 = 0.02778$ cm и $h \approx 1.775$ cm on the grid with $L_0 = 0.02083$ cm.

The influence of L_0 on the dependence $h(Z)$ on a fixed grid is shown in the fig. 4.b. One can see that when L_0 increases it results into an increase of the the light-to-heavy fluid penetration depth by a constant value Δh, which weakly depends on the ampoule's path Z.

Pulse acceleration.

The numerical results with the ampoule's pulse acceleration are shown in the fig. 5.a and 5.b. The fig. 5.a shows that if the number of points in the differencing grid is increased by a factor of 1.5 (respectively, L_0 decreases by a factor of 1.5) h at the end of calculations decreases by about 5.6%, and a twofold increase results into h at the end decreasing by about 16%. In this case there is a slight dependence of the growth rate dh/dZ on L_0 through out the calculation.

The fig. 5.b shows the influence of L_0 on the dependence $h(Z)$ on a fixed grid. One can see that the most pronounced dependence of dh/dZ on L_0 is observed at the beginning of TM calculations. At the phase of the developed TM the influence of L_0 becomes weaker. Comparing the results obtained for the constant, decreasing, increasing and pulse accelerations, one can note that the influence of L_0 on the dependence $h(Z)$ is the most pronounced for the pulse acceleration.

CONCLUSION.

Numerical simulations of Dimonte's experiments[6] on Raleigh-Taylor mixing of two molecularly immiscible fluids have been performed with the VIKHR technique. The calculations have been performed for four ampoule acceleration laws. There is satisfactory agreement with the data [6]. Thus, we can state that V.V.Nikiforov's TM model provides adequate treatment of turbulent flow evolution in absence of shock waves.

REFERENCES.

1. *V.A. Andronov, V.I. Kozlov, V.V. Nikiforov, A.N. Razin, Yu.A. Yudin* Turbulent mixing calculation technique for 1D flows (the VIKHR technique) // Voprosy Atomnoy Nauki i Techniki. Series: Mathematical modeling of physical processes. 1994, issue 2, p. 59-64.
2. *V.A. Andronov, V.V. Nikiforov* Turbulence evolution calculations with an axially symmetric strain // Voprosy Atomnoy Nauki i Techniki. Series: Theoretical and applied physics. 1990, issue 1, p. 34-36.
3. *V.A.Andronov, S.M.Bakhrakh, E.E.Meshkov, V.V.Nikiforov, A.V.Pevnitsky, A.I.Tolshmyakov* An experimental study and numerical simulations of turbulent mixing in 1D flows // Doklady AN SSSR. 1982, vol. 264, № 1, p. 76-82.
4. *V.V.Nikiforov, V.A.Andronov, A.N.Razin* Turbulent mixing zone evolution under shock impact // Doklady AN SSSR. 1995, vol. 343, # 3, p. 323-325.
5. *V.A.Andronov, S.A.Bel'kov, A.V.Bessarab et.al.* Investigation of turbulent mixing in thin layers with different densities during laser acceleration of plane multilayer targets at the ISKRA-4 facility// JETF, 1997, vol. 111, issue 3, p. 882-888.
6. *Dimonte Guy, Schneider Marilyn.* Turbulent Rayleigh-Taylor instability experiments with variable acceleration // Physical Review E, 1996, v. 54, № 4, p.3740-3743.
7. *Kuchtrenko Yu.A., Shibarshov L.I., Chitaikin V.I., Balabin S.I., Pylaev A.P.* Experimental study of the gravitational turbulent mixing self-similar mode. 3rd International Workshop on the physics of compressible turbulent mixing (Abbey of Royaumont, France), 1991, p. 427.

8. *D.L. Youngs*, Physica 12 D, 32, 1984.

9. *K.I. Read* Experimental investigation of turbulent mixing by Rayleigh-Taylor instability, Part 1. // Atomic Weapons Research Establishment, Foulness, England, 1984.

10. *V.V.Nikiforov* Turbulent mixing at an interface of different-density fluids. // Voprosy Atomnoy Nauki i Techniki. Series: Theoretical and applied physics. 1985, issue 1, p. 3÷8.

11. *V.V.Nikiforov* Calculations of gravitational turbulent mixing in non-self-similar flows // Voprosy Atomnoy Nauki i Techniki. Series: Theoretical and applied physics. 1993, issue 1, c. 3-13.

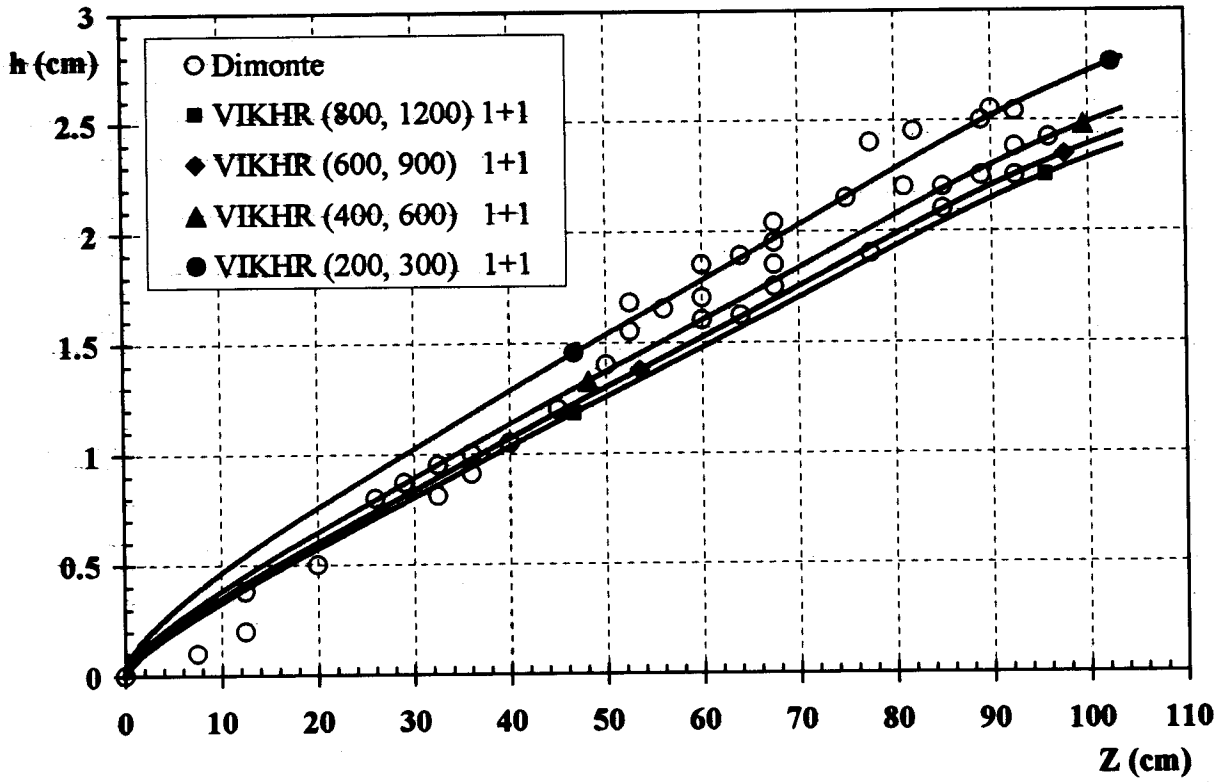

Fig. 2,a. Constant acceleration: calculations with a sequence of refined grids. (Initial density fluctuations are set in one point to the left and one point to the right of the interface.)

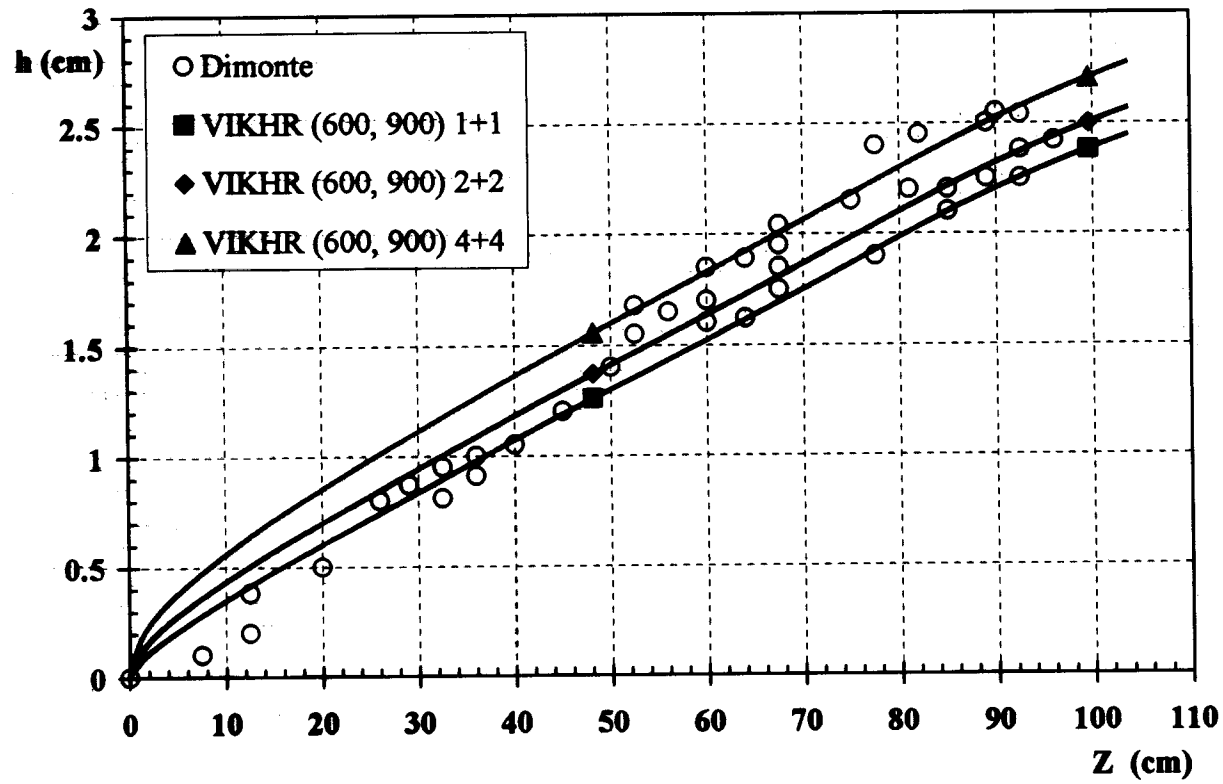

Fig. 2,b Constant acceleration: calculations with variable initial zone width L_0 on a fixed grid. (L_0 is given by the number of numerical points to the left and to the right of the interface where the initial density fluctuations are set.)

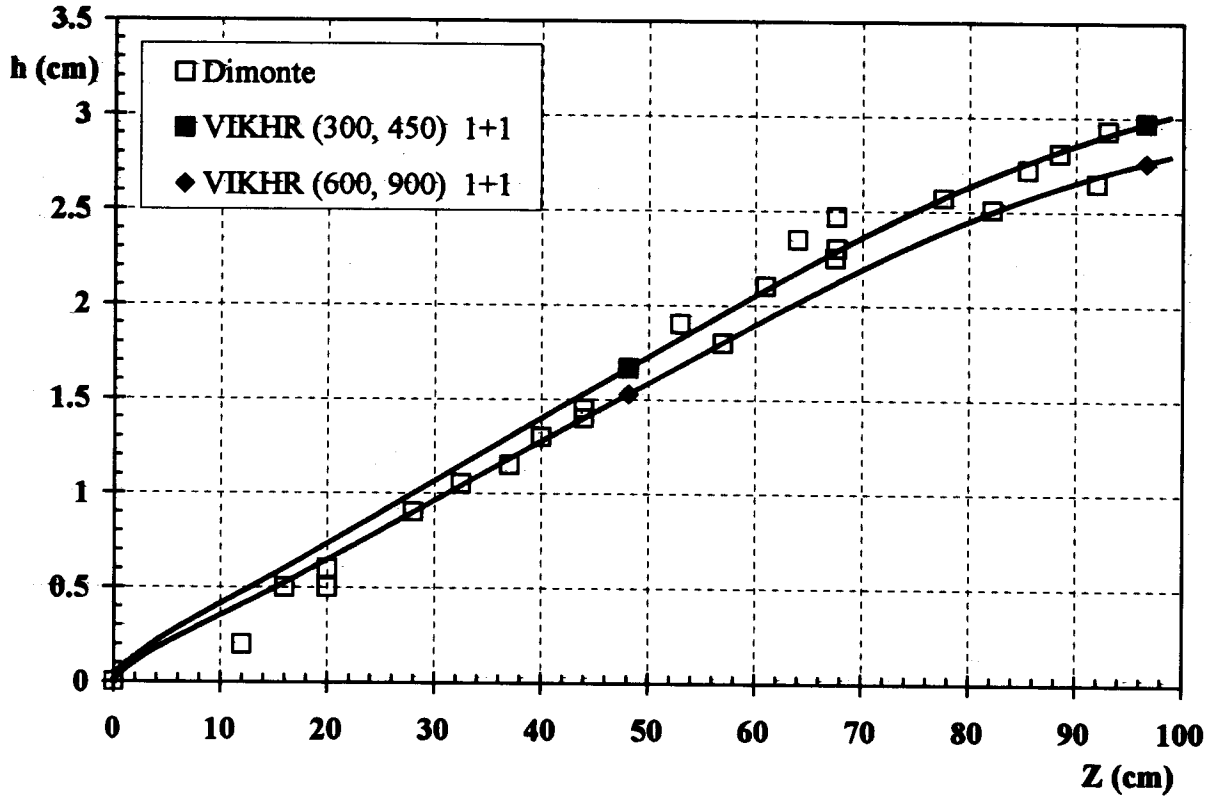

Fig. 3,a. Increasing acceleration: calculations with a sequence of refined grids. (Initial density fluctuations are set in one point to the left and one point to the right of the interface.)

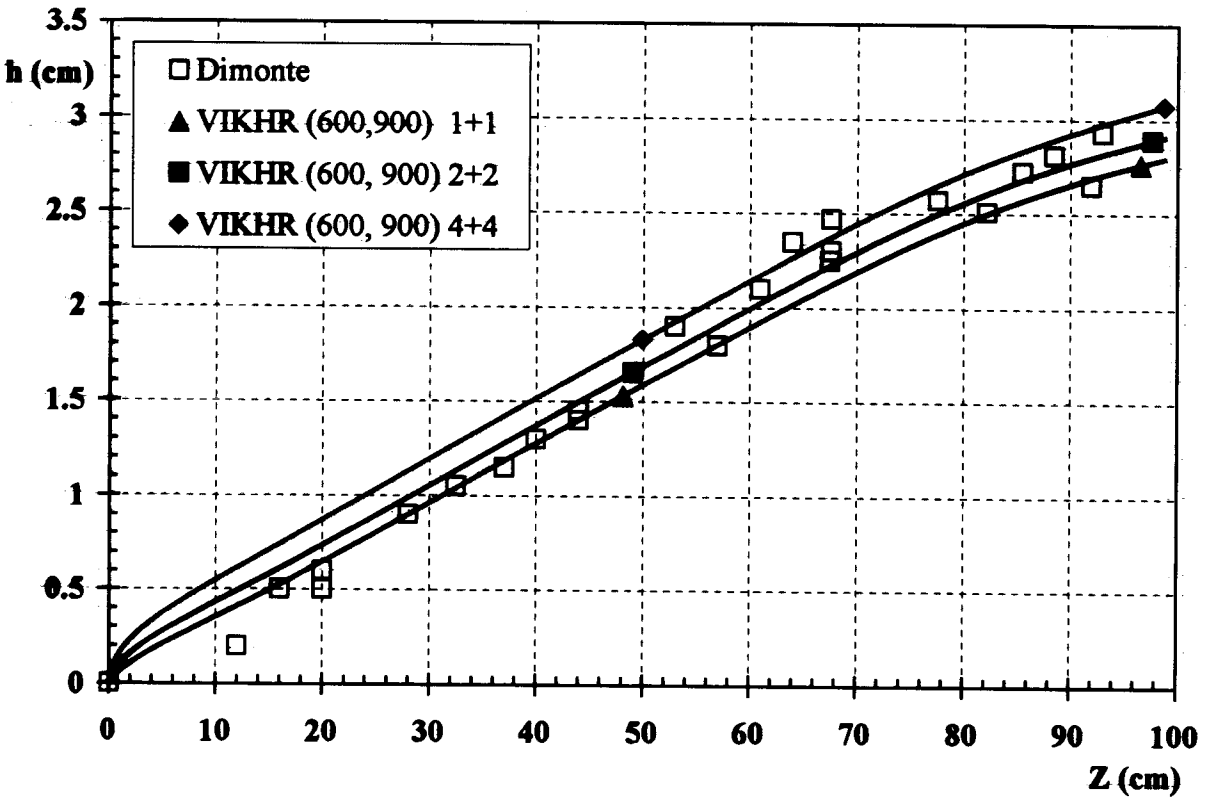

Fig. 3,b. Increasing acceleration: calculations with variable initial zone width L0 on a fixed grid. (L_0 is given by the number of numerical points to the left and to the right of the interface where the initial density fluctuations are set.)

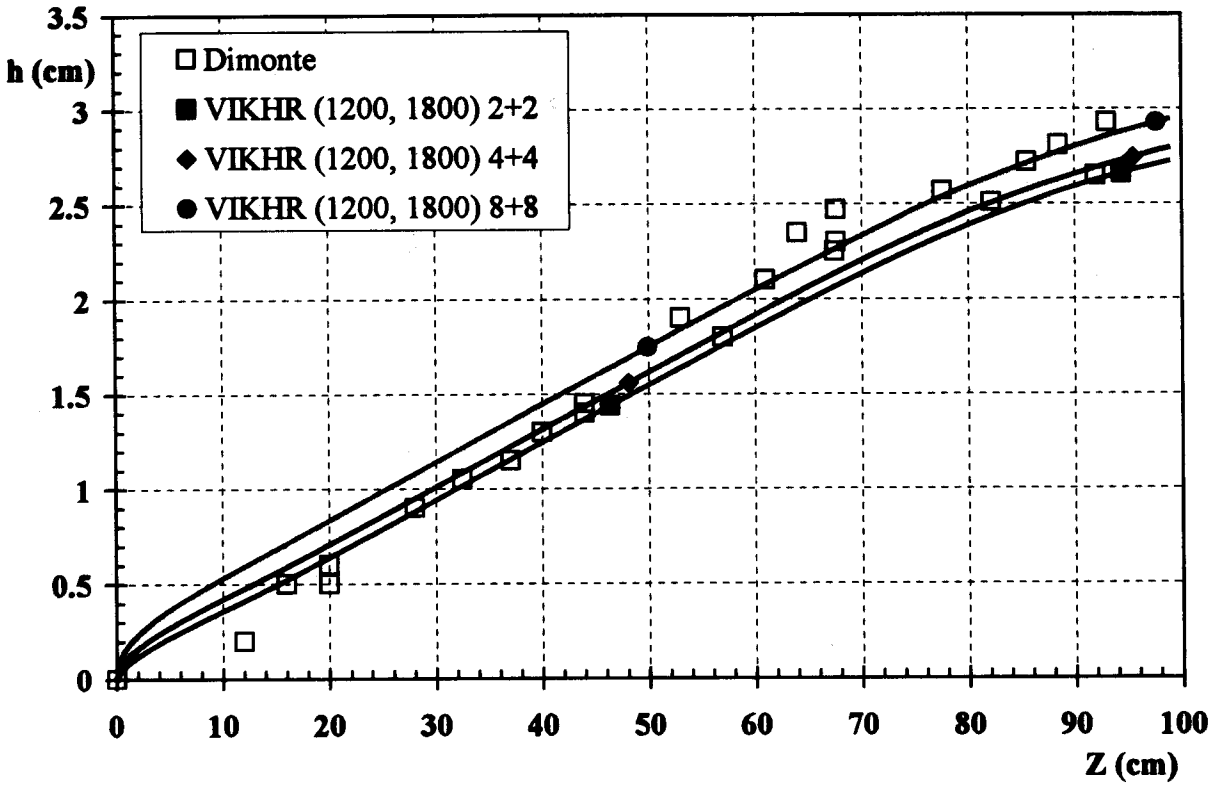

Fig. 3,c. Increasing acceleration: calculations similar to those shown in the fig. 3.b, but the number of numerical points increased twofold.

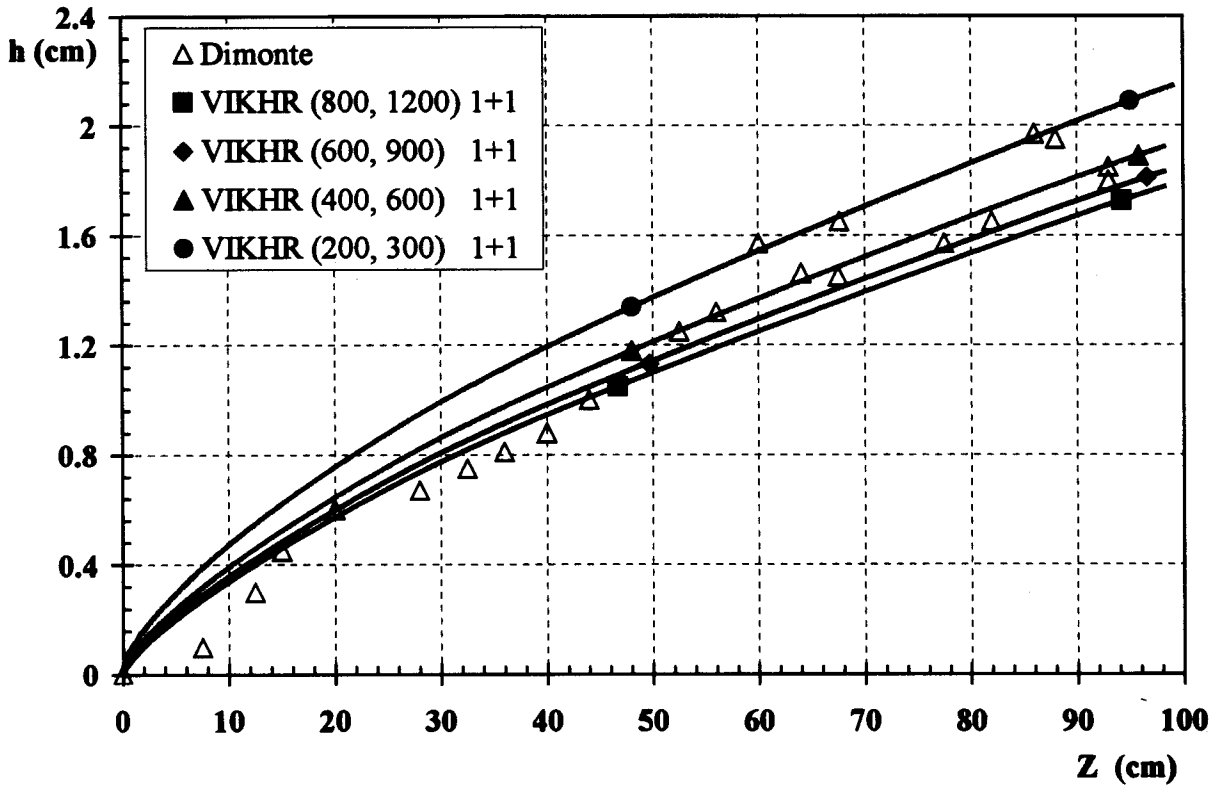

Fig. 4,a. Decreasing acceleration: calculations with a sequence of refined grids. (Initial density fluctuations are set in one point to the left and one point to the right of the interface.)

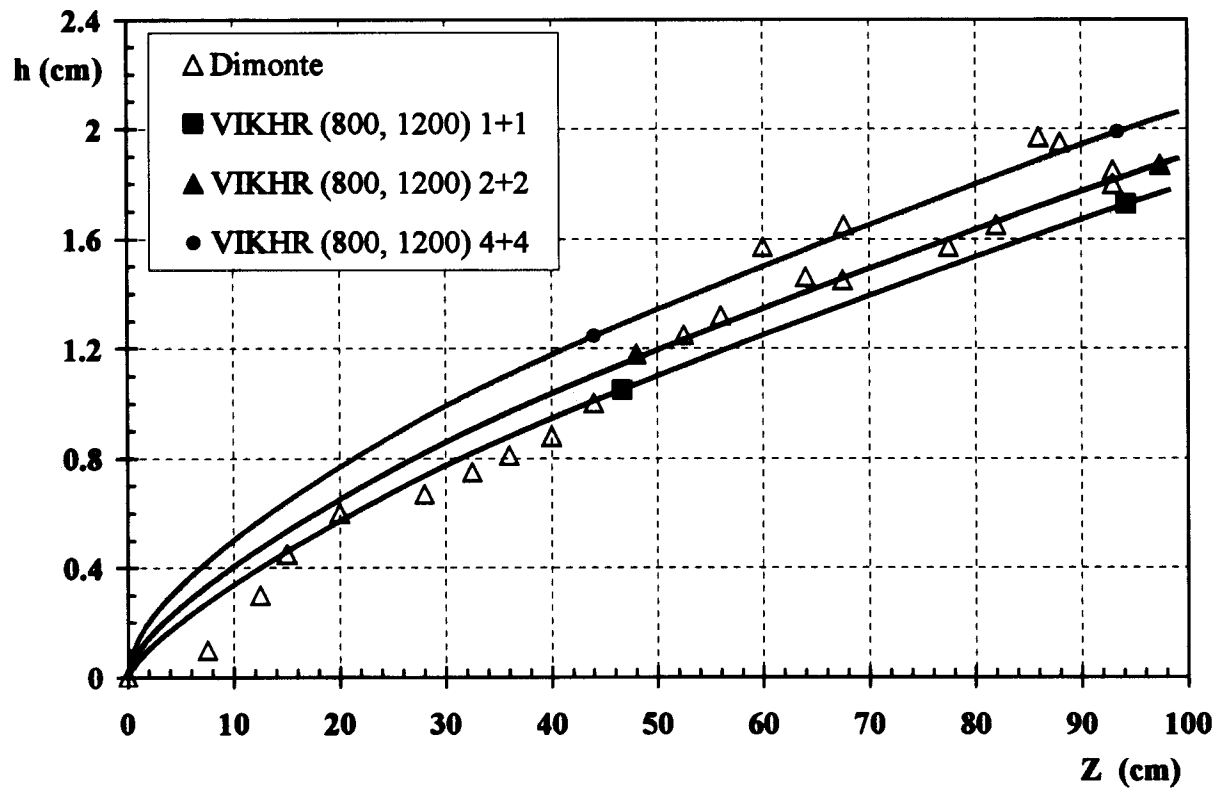

Fig. 4,b. Decreasing acceleration: calculations with variable initial zone width L_0 on a fixed grid. (L_0 is given by the number of numerical points to the left and to the right of the interface where the initial density fluctuations are set.)

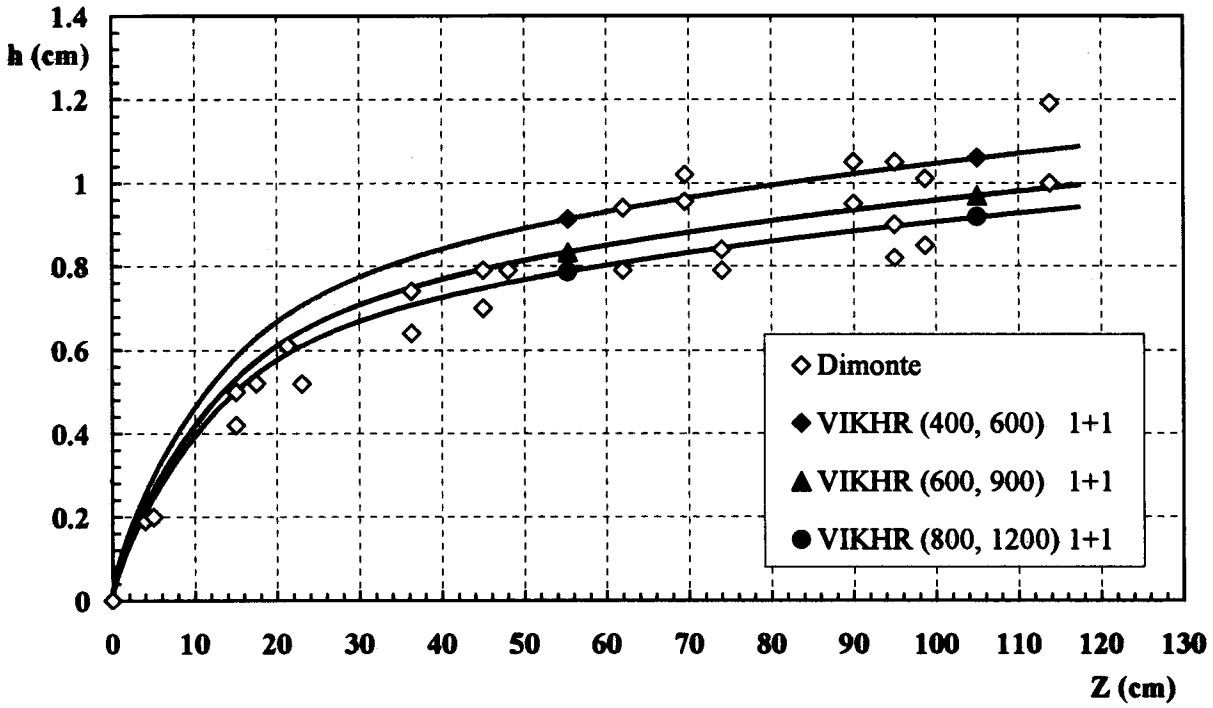

Fig. 5,a. Pulse acceleration: calculations with a sequence of refined grids. (Initial density fluctuations are set in one point to the left and one point to the right of the interface.).

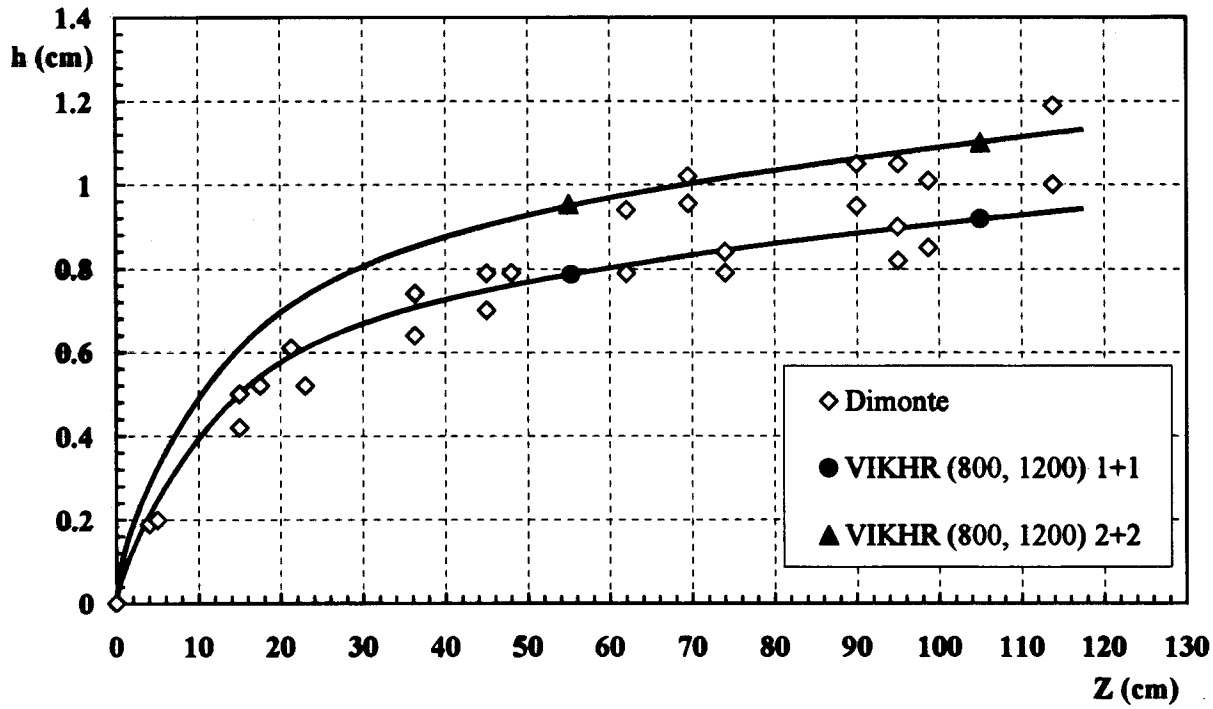

Fig. 5,b. Pulse acceleration: calculations with variable initial zone width L_0 on a fixed grid. (L_0 is given by the number of numerical points to the left and to the right of the interface where the initial density fluctuations are set.)